



HAL
open science

Carbonate weathering, CO₂ redistribution, and Neogene CCD and pCO₂ evolution

Louis A. Derry

► **To cite this version:**

Louis A. Derry. Carbonate weathering, CO₂ redistribution, and Neogene CCD and pCO₂ evolution. Earth and Planetary Science Letters, 2022, 597, 10.1016/j.epsl.2022.117801 . insu-03824248

HAL Id: insu-03824248

<https://insu.hal.science/insu-03824248>

Submitted on 21 Oct 2022

HAL is a multi-disciplinary open access archive for the deposit and dissemination of scientific research documents, whether they are published or not. The documents may come from teaching and research institutions in France or abroad, or from public or private research centers.

L'archive ouverte pluridisciplinaire **HAL**, est destinée au dépôt et à la diffusion de documents scientifiques de niveau recherche, publiés ou non, émanant des établissements d'enseignement et de recherche français ou étrangers, des laboratoires publics ou privés.



Distributed under a Creative Commons Attribution - NonCommercial 4.0 International License



Carbonate weathering, CO₂ redistribution, and Neogene CCD and pCO₂ evolution

Louis A. Derry

Institut de Physique de Globe de Paris (IPGP), Cornell University, Department of Earth and Atmospheric Sciences, 1 rue Jussieu, 75005 Paris, France



ARTICLE INFO

Article history:

Received 29 March 2022

Received in revised form 26 August 2022

Accepted 28 August 2022

Available online 16 September 2022

Editor: A. Jacobson

Keywords:

carbonate compensation depth

CCD

pCO₂

Neogene

carbonate weathering

ABSTRACT

The carbonate compensation depth (CCD), $\delta^{13}\text{C}$ of marine carbonate, atmospheric pCO₂ and major ion composition of seawater provide constraints on how geological carbon cycle processes evolved over the Neogene. I use simple models and the LOSCAR ocean carbon system model to assess what changes in carbon fluxes to the ocean are necessary to explain observations since the early Miocene. The calculations consider estimates of early Miocene seawater temperatures and ion composition and a range of possible pCO₂. Changes in shelf-basin partition could explain up to $\approx 45\%$ the observed CCD deepening. Increased carbonate flux (likely range $28 \pm 12\%$) to the oceans is necessary to explain the rest. Despite changes in pCO₂ from early Miocene values of 450–900 ppm to a pre-anthropogenic value of 280 ppm, the size of the total ocean-atmosphere carbon reservoir shows only moderate or no net change, implying that weathering and/or organic carbon burial result in little net CO₂ consumption. Decreasing Ca⁺⁺ and increasing deepwater carbonate saturation over the Neogene require a large increase in deepwater CO₃⁼ and leads to decreasing DIC/TALK which is the main driver for falling pCO₂. The primary driver of pCO₂ reduction is redistribution of CO₂ from the atmosphere to the oceans, not net removal of CO₂ from excess silicate weathering or organic carbon burial. The main impact of tectonic perturbation of the carbon cycle during the Neogene is to enhance carbonate weathering while only weakly affecting the net balance of degassing vs. silicate weathering or kerogen oxidation vs. organic carbon burial.

© 2022 The Author. Published by Elsevier B.V. This is an open access article under the CC BY-NC license (<http://creativecommons.org/licenses/by-nc/4.0/>).

1. Introduction

Understanding the nature, rates, and causes of changes in global climate and carbon cycling that have occurred over the last 20–25 Ma remains a major challenge in the Earth sciences (Steinthorsdottir et al., 2021). Proxy approaches have been developed to provide insight into some of the relevant processes and how they may have evolved through time. Tracer approaches are valuable in that they can be sensitive to various aspects of the geochemical cycle, but their relationships to carbon fluxes are not always direct, may change over time and can be difficult to evaluate independently. This study instead focuses on parameters that most directly reflect carbon fluxes to address broad scale changes in the Earth system since the early Miocene. These include the carbonate compensation depth (CCD) as a record of carbonate deposition in the oceans, atmospheric pCO₂ reconstructions, the major ion composition of seawater, and the $\delta^{13}\text{C}$ of marine carbonates. The goal of this study is not to produce a detailed time series of carbon flux estimates over the Neogene. Instead, I seek to evaluate how carbon input and removal processes could have changed since the early

Miocene to be consistent with observed records of the CCD, pCO₂, $\delta^{13}\text{C}$ and Ca-Mg-SO₄?

2.

2.1. Carbonate accumulation and the carbonate compensation depth

The carbonate compensation depth (CCD) is the depth where the rate of carbonate dissolution is balanced by the rate of supply of sinking carbonate minerals to marine surface sediments, i.e. where net accumulation reaches zero. The position of the CCD can be determined for the past by quantifying changes in carbonate accumulation in dated sediment cores and reconstructing their paleodepth at the time of deposition and is an indicator of carbonate flux to the deep sea. Well above the CCD carbonate preservation and carbonate fraction in sediments is high. Above the CCD but below this zone of high saturation state is a transition zone (0–1000 m thick), where the carbonate fraction in sediments declines and accumulation rates taper off toward the CCD. Absent large changes in the depth-carbonate fraction relationship a deepening of the CCD imply increased carbonate deposition flux in the deep sea. Nearly all assessments of the late Cenozoic history of the CCD agree at least qualitatively with an overall deepening

E-mail address: derry@cornell.edu.

Table 1

a) Estimates of marine carbonate burial fluxes (Tmol yr^{-1}) for early Miocene and modern pre-anthropogenic conditions. b) Representative modern marine system Ca fluxes. Model simulations here use a steady silicate weathering input = 7.1 Tmol yr^{-1} , and a modern carbonate input (weathering + ion exchange + hydrothermal) of 18 Tmol yr^{-1} .

Carbonate burial rate estimates	Modern	Early Miocene
Berner and Berner, 2012	24	17
Berner and Mackenzie, 2011 (ave)	21	20
Opdyke and Wilkinson, 1988	29	19
Dutkiewicz et al., 2018	25.8	18.8
Suchéras-Marx and Henderiks, 2014	6 - 10	6 - 10
Iglesias-Rodriguez et al., 2002	26.5-29.8	
Boudreau et al., 2019	14	11
Inputs 0 Ma		
Tmol yr^{-1}		
Rivers: silicate Ca, Mg	7.1	
Rivers: carbonate	15.2	
Hydrothermal ex OC	1.8	
Cation exchange	0.9	
total input	25	

from 25 Ma to the present (Van Andel, 1975; Delaney and Boyle, 1988; Peterson and Backman, 1990; Boss and Wilkinson, 1991; Lyle, 2003; Tyrrell and Zeebe, 2004; Campbell et al., 2018). One exception is Pällike et al., 2012 who show no clear long-term trend over this interval. However, Campbell et al., 2018 were unable to reproduce this result despite working with the same core data, and the source of the discrepancy remains unclear. Other studies that do not rely, or rely only partly, on CCD reconstructions, also find substantially increased deep sea and overall carbonate deposition over this interval (Opdyke and Wilkinson, 1988; Delaney and Boyle, 1988; Mackenzie and Morse, 1992; Berner and Berner, 2012; Berner and Mackenzie, 2011; Dutkiewicz et al., 2018). Some published estimates of CaCO_3 sedimentation for both the modern and early Miocene are summarized in Table 1a.

Input of carbonate to the oceans includes (1) net Ca and Mg exchange during alteration of the oceanic crust, (2) ion exchange (such as Ca^{++} for $\text{Na}^+ + \text{K}^+$) and (3) river inputs. River inputs can further be divided into Ca and Mg from silicate weathering and from carbonate weathering. Removal is dominated by sedimentation of calcium carbonate. For present purposes an exact budget is unnecessary. The focus of this exercise is to evaluate plausible changes in the CaCO_3 budgets over time rather than absolute fluxes. The net hydrothermal exchange flux with the oceanic crust (OC) is estimated from the difference between Mg uptake and Ca release (Berner and Berner, 2012). Ca, Mg silicate weathering fluxes are from Gaillardet et al. (1999). The equivalent Ca-silicate weathering flux is 7.1 Tmol yr^{-1} ($\text{Tmol} = 10^{12} \text{ mol}$). The difference between the total silicate weathering flux ($11.7 \text{ Tmol yr}^{-1}$) and the Ca, Mg silicate flux is $4.6 \text{ Tmol C yr}^{-1}$, which approximates the $\text{Na}^+ + \text{K}^+$ flux. France-Lanord and Derry (1997) estimated that 15% of $\text{Na}^+ + \text{K}^+$ could exchange for Ca^{++} , implying a Ca^{++} exchange flux $\approx 0.7 \text{ Tmol yr}^{-1}$. Berner and Berner (2012) give a value $\approx 0.9 \text{ Tmol yr}^{-1}$ for the Ca^{++} exchange flux. For the carbonate weathering flux we adopt a value of $15.2 \text{ Tmol yr}^{-1}$ (compare to 12.3 in Gaillardet and 13.8 in Berner and Berner, 2012). This higher value is chosen for the convenience of yielding approximate steady state with total carbonate deposition values from Iglesias-Rodriguez et al. (2002), Berner and Berner (2012) and Dutkiewicz et al., 2018 and ($\approx 25 \text{ Tmol yr}^{-1}$). These values yield a residence time for oceanic Ca with respect to river inputs $\approx 0.65 \text{ Ma}$.

Campbell et al. (2018) recalculated the CCD for the equatorial Pacific from the PEAT transect (IODP 320/321) along with additional data from nearby ODP sites. They calculated paleodepth considering not only simple thermal subsidence as a function of

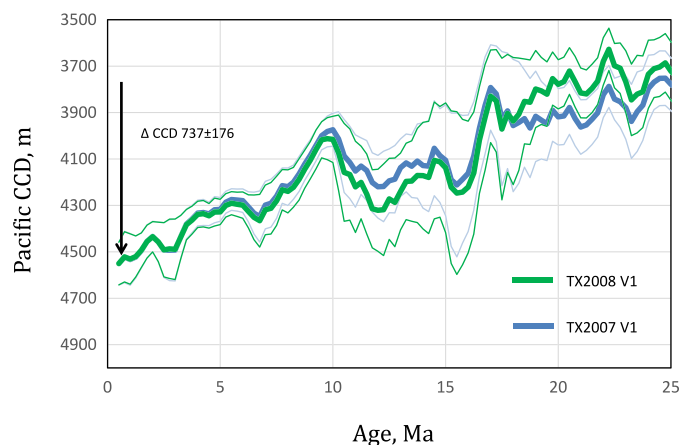


Fig. 1. Pacific CCD reconstructed after correction for dynamic topography by Campbell et al., 2018. TX2007 V1 (blue line) TX 2008 V1 (green line). Thin lines are 2σ uncertainties. Using the reconstruction in Campbell et al. (2018) the mean of the CCD estimates for the 20–21.5 Ma interval is used as a starting condition for the early Miocene and compared to the 0.5 Ma results as an approximation for the modern CCD (the last time slice computed by Campbell et al.). The primary goal is to evaluate the change in the CCD rather than the absolute values. The Pacific CCD deepens from 3813 to 4550 m, for a $\Delta\text{CCD} = 737^{+176}/_{-164} \text{ m}$ using the average of TX2007/08 V1 models.

lithosphere age, but also changes in dynamic topography resulting from mantle convection effects. The East Pacific Rise region has been shown to have significant mantle buoyancy anomalies and the proximity of some of the PEAT sites to the East Pacific Rise indicates that these effects can be significant for paleodepth reconstruction (Rowley et al., 2016). Campbell et al., 2018 estimated that these effects were of the order of hundreds of meters over the last 30 Ma. They used these modified paleodepth reconstructions to recompute the equatorial Pacific CCD. Two density and two viscosity models were used. The density models TX2007 and TX2008 yield similar results for a given viscosity model. Rowley et al. (2016) evaluated several density and viscosity models and found that the V1 viscosity model yielded a better fit to global geodynamic indicators; those results are used here (Fig. 1). The Campbell et al., 2018 CCD record is used here because it includes the high-resolution PEAT core data from the equatorial Pacific, makes an important correction for dynamic topography, uses a Type II regression, and the data, methods and uncertainties are clearly documented. The Indian Ocean CCD is not well constrained prior to 22 Ma, but Campbell et al. (2018) found the overall increase in depth from 20 Ma to 0.5 Ma ranged from 1208 to 1405 m with early Miocene uncertainties on the order of $\pm 300 \text{ m}$. I note this larger increase in depth of the Indian CCD but use the better constrained Pacific data set to evaluate changes in the oceanic C cycle. An updated South Atlantic CCD record shows a deepening of $\approx 700 \pm 300 \text{ m}$ since the early Miocene (Dutkiewicz and Müller, 2021).

Changing sea level can impact the CCD by changing the shelf-basin partitioning of carbonate (Opdyke and Wilkinson, 1988). An approximate estimate of this effect can be obtained from global hypsometry. From the ETOPO1 data (Amante and Eakins, 2009) a 50 m sea level fall implies a reduction in shelf area of $-13.5 \times 10^6 \text{ km}^2$, or 50% of shelf area taking a conventional limit of 200 m depth for the global shelf environment. Assuming that shelf area and carbonate deposition scale simply, this would imply a similar reduction in shelf carbonate burial (Cartapanis et al., 2018). While the extremes vary more widely, the smoothed sea level curve of Miller et al. (2020) varies by about 70 m from the maximum during the MMCO to the mid-Pleistocene, and by about 40 m from the early Miocene. A deepening of the global CCD from 3810 to 4550 m implies an increase in carbonate deposition over $83.5 \times 10^6 \text{ km}^2$,

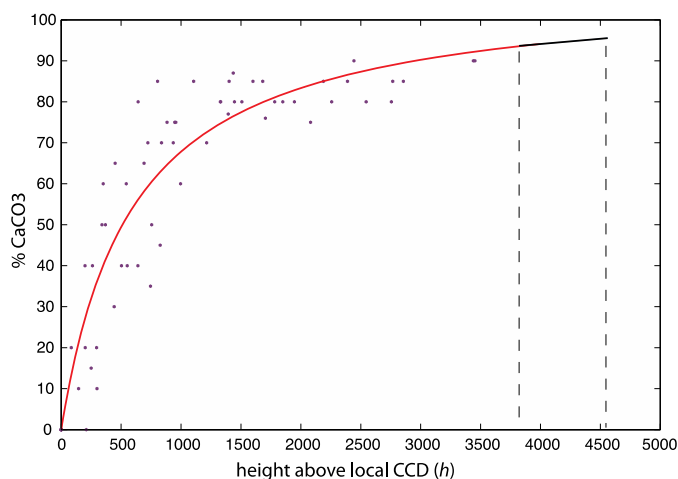


Fig. 2. Marine sediment carbonate fraction as a function of height above local CCD. Data are from Archer (1996) and include Pacific and Atlantic sites. The arbitrary function fit to the data was chosen for simplicity (see SI). The increase in area under the curve for a CCD deepening of 740 m is 25%, illustrated by the dashed lines.

an area about six times larger than the decrease in shelf deposition area resulting from a 50 m sea level fall.

One way to conceptualize the relationship between a changing CCD and carbonate accumulation is to consider the impacts at shallower depths. As the CCD deepens, the transition zone also deepens, extending the shallower depth interval over which the carbonate fraction of sediments should be high. This may be visualized by plotting the carbonate fraction as a function of height above the local CCD, creating a stack of carbonate vs. depth records normalized for local variations in the CCD (Fig. 2). The carbonate-fraction-depth relationship can be integrated to estimate changes in overall carbonate deposition for a given change in the CCD. An increase in CCD depth of 740 m implies an increase in carbonate deposition of $\approx 25\%$. This depends on having a relatively constant relationship between depth and carbonate fraction, i.e. the thickness of the transition zone. A related projection was used by Boudreau and Luo (2017) and like them I take this assumption as a reasonable starting point, noting that data from different ocean basins with different water column saturation profiles all collapse to similar profiles when plotted relative to the local CCD. However, Suchéras-Marx and Henderiks (2014) and Si and Rosenthal (2019) argued for decreased net accumulation of carbonate at mid-depths since ca. 4 Ma, impacting the transition zone, despite an inferred constant CCD (see SI). In contrast, Farrell and Prell (1991), working in the eastern equatorial Pacific, found a clear increase in CaCO_3 accumulation since 4 Ma. The total carbonate accumulation rate during the Miocene derived by Suchéras-Marx and Henderiks, 2014 (Table 1) is markedly lower than other estimates, possibly pointing to the difficulties in scaling up globally using a relatively small number of site-specific studies.

2.2. LOSCAR simulations of CCD

One goal of the present study is to evaluate the potential impacts of change in alkalinity fluxes, sea level, atmospheric CO_2 , temperatures, and the major ion composition of seawater on the CCD. I also consider the available constraints on atmospheric pCO_2 and the benthic $\delta^{13}\text{C}$ record. I carried out a set of representative experiments with the LOSCAR oceanic carbon cycle model (Zeebe, 2012). LOSCAR computes the distribution of carbon species in 10 oceanic boxes, and carbonate deposition in the major ocean basins, including the position of the CCD. Parameters needed for LOSCAR include water mass temperature and major ion chemistry of the oceans (Ca^{++} , Mg^{++} and $\text{SO}_4^{=}$) because of their impact on

Table 2

LOSCAR parameters. Units: T °C, ion concentrations mM, pCO_2 ppmv, Fvc and FINC Tmol C yr^{-1} . FSHELF is non-dimensional.

	Modern	Miocene
Surface T	20	25
Intermediate T	10	15
Deep and Hi Lat T	2	7
Ca^{++}	10.3	14.0
Mg^{++}	53.0	43.0
$\text{SO}_4^{=}$	28.2	22.0
pCO_2	280	450–900
Fvc	7.1	7.1
FINC	18	12–18
Fshelf	1.0	1–4

carbonate equilibria. It also requires specification of steady state rates of volcanic degassing of CO_2 and of carbonate weathering. Through a simple feedback, silicate weathering rates adjust over time until the weathering of Ca-silicates equals CO_2 degassing. The Ca-carbonate weathering flux can be allowed to adjust to a specified steady state value, where the model changes the weathering flux as $f(\text{pCO}_2)$ until the weathering flux = steady state value. Alternatively, the dependence of the carbonate weathering flux on pCO_2 can be suppressed and given a fixed value. At steady state these two approaches are equivalent. The carbonate input term FINC here is defined as the sum of the inputs from carbonate weathering, cation exchange and hydrothermal exchange (modern value 18 Tmol yr^{-1} , Table 1). A scaling parameter FSHELF changes the distribution of carbonate sedimentation between the shelf and abyssal environment; a value of 1 represents modern conditions. Zeebe et al. (2009) used a value of $\text{FSHELF} = 4.5$ to represent PETM conditions which were ice-free and included extensive Tethyan shelf environments. Here I explore how changes in several key parameters impact the computed CCD and distribution of DIC in the oceans under plausible early Miocene scenarios compared to simulations using modern (default) conditions. As noted above, the Pacific ocean CCD is taken as the primary benchmark since it is better constrained than the CCD for other regions.

2.2.1. Choosing initial mass balances

Table 1 lists estimates of modern Ca^{++} equivalent fluxes to the oceans. The steady state Ca-silicate weathering flux is set as the LOSCAR parameter for volcanic CO_2 input $f\text{-vc} = 7.1 \text{ Tmol yr}^{-1}$. For Miocene simulations $f\text{-vc}$ is constant while FINC is varied (Table 2). The shelf-basin parameter FSHELF is varied from 1 (modern) to 4, where higher values would be associated with higher sea levels and consequently higher shelf/abyssal deposition ratios. Using the current distribution of shelf and deep deposition from Iglesias-Rodríguez et al., 2002, values of FSHELF from 1 to 4 imply a change in shelf/abyssal deposition ratio from a modern value ≈ 1.1 to up to as high as 4.6 for the early Miocene (see SI), although the data on shelf vs. deep carbonate accumulation remain uncertain and so this is an approximate equivalence.

2.2.2. Ocean temperatures and major ion composition

Modern values are the default values from LOSCAR. Early Miocene SSTs are from Burls et al., 2021, and deep water T from Lear et al., 2015 and Cramer et al., 2011. High latitude T is equal to deep water T (see SI). Intermediate water T was estimated between SSTs and deep water. For $[\text{Ca}^{++}]$, $[\text{Mg}^{++}]$ and $[\text{SO}_4^{=}]$ are estimated from the data of Horita et al., 2002 and Brennan et al., 2013, yielding mid-early Miocene Mg/Ca ratios that agree with Coggon et al., 2010; Rausch et al., 2012 and Gothmann et al., 2015 (see SI). The question of how best to address the impact of changes

in the major ion chemistry of seawater on $\text{CO}_2\text{-H}_2\text{O-Ca}$ equilibria is not straightforward (Hain et al., 2015; Zeebe and Tyrrell, 2019). The simulations here were run using the adjustment to stoichiometric constants described in Zeebe and Tyrrell (2019) which is a set of linear approximations to an ion pairing model. While there are uncertainties for early Miocene ocean temperatures and major ion composition, in the interests of simplicity those values were held constant for all early Miocene simulations. For pCO_2 , in addition to the modern pre-anthropogenic 280 ppm value, Miocene simulations were run at 450, 600 and 900 ppm. This range approximates that given in Rae et al. (2021).

LOSCAR was run to steady state so that the silicate weathering flux $F(\text{Ca-silicate}) = F_{\text{vc}}$ for all simulations. The carbonate weathering feedback was removed (set $n_{\text{cc}} = 0$) so that FINC remained constant throughout a given run.

3. Results

LOSCAR was run with the default modern conditions (Table 2) as a benchmark. The combined effects of changing ocean temperatures and chemistry were tested by holding silicate and carbonate weathering fluxes constant (at steady state) at the “modern” values. The FSHELF parameter was also held constant at 1.

The default (modern) settings produce a Pacific CCD = 4299 m, too shallow by 252 m relative to the value estimated by Campbell et al., 2018. The computed modern CCD for the Indian Ocean is 4837 m, in better agreement with Campbell et al. (4800 m). Relative to observations from the modern deep Pacific and Indian oceans (3.5 km depth) summarized by Zeebe and Westbroek (2003) DIC, $\text{CO}_3^{=}$ and pH are slightly overestimated.

Increasing FINC to 23 Tmol yr^{-1} largely eliminates the model-data discrepancy in the Pacific CCD, but at the cost of substantially increasing it for DIC, $\text{CO}_3^{=}$ and pH. Decreasing FINC improves the agreement with the water column parameters but at the cost of rapidly degrading the CCD fit by making the CCD much too shallow. Here we are interested in *changes* from a given set of conditions and so the results using the default modern model input should be acceptable as a basis for comparison with results from the same model but different boundary conditions. The LOSCAR model as initialized here does not do an effective job of capturing the deeper Indian ocean CCD although it does predict a deepening of the Indian CCD. It is unclear if the mismatch between the depth of Indian CCD and the model results is a consequence of the less well characterized CCD there, or possibly circulation effects that are not captured in the LOSCAR simulations, or some other reason.

3.1. Dependence of CCD on ocean temperature and chemistry

The effects of water temperature and chemistry on the computed CCD were tested independently and together. The effects of T and chemistry are not additive. The differences between runs with warmer ocean conditions and the default resulted in slight shoaling ≤ 25 m. For changes in chemistry at 280 ppm the CCD shoaled by 84 m while at 450 ppm the CCD deepened by -45 m. Changes in both temperature and chemistry to estimated early Miocene conditions resulted in slight shoaling ≤ 48 m for $\text{pCO}_2 = 280$ to 900 ppm (Figure S3). These examples indicate that changes in water temperature and major ion composition alone have effects on the position of the CCD on the order of 10's of meters only, regardless of pCO_2 , and despite significant impacts on deep water ($\text{CO}_3^{=}$).

3.2. Dependence of CCD on shelf-basin partitioning

Changing shelf – basin partitioning has a larger impact. With early Miocene T and chemistry and FINC = 18 (modern), FSHELF

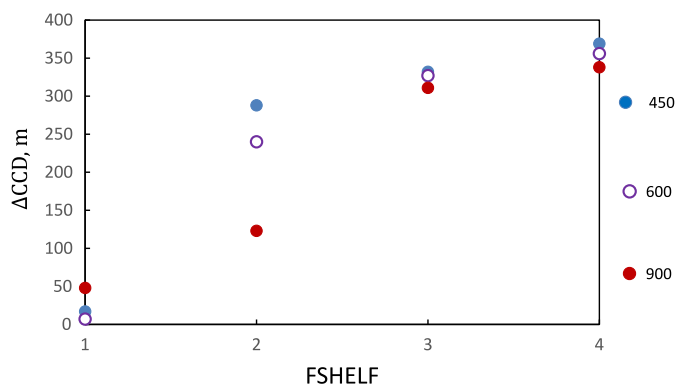


Fig. 3. Change in CCD relative to modern case for FINC held constant at 18 Tmol yr^{-1} and FSHELF varied from 1 (modern) to 4. Increasing shelf deposition leads to less carbonate delivery to the deep sea, shoaling the CCD. pCO_2 varies from 450–900 ppm.

was increased from 1 to 4 for different pCO_2 , implying a change in the ratio of shelf to basin deposition of a factor of 4. The CCD shoals by up to 370 m for 450 ppm CO_2 (Fig. 3). Values of FSHELF ≥ 4 imply ice free conditions and are not likely to be applicable to the early Miocene (Miller et al., 2020). However even with this unrealistically large value the combined changes in ocean temperature, chemistry and shelf-basin partitioning only explain half, at most, of the observed change in the CCD since the early Miocene. This conclusion differs from that of Komar and Zeebe (2021) in part because of the chosen Neogene CCD history.

3.3. Combined impacts of shelf-basin partitioning and carbonate input fluxes

A series of experiments for different shelf deposition and pCO_2 (FSHELF = 2 to 4, $\text{pCO}_2 = 450$ to 900) for early Miocene T and chemistry while allowing carbonate input to vary show that the combination of changes in shelf-basin partitioning and increasing carbonate weathering flux can match the observed deepening in the Pacific CCD. These numerical experiments do not cover all possible combinations of input flux, water mass properties or shelf deposition, but give a useful view of potential differences between early Miocene and modern conditions necessary to produce the observed changes in the CCD (see Fig. 4).

The intersection of the computed CCD with the observed range implies an increase in total carbonate supply to the oceans of about $28 \pm 12\%$ (full range 9% to 50%), depending on the parameter value for shelf deposition and pCO_2 . It is important to note that, while FINC is the input parameter varied here the distribution of carbonate between the ocean reservoirs does not depend on whether FINC or F_{vc} is varied. This result is fully consistent with the simple hypsometric calculation above using the change in sedimentary carbonate content with respect to the local CCD (Fig. 2). It is also consistent with previous estimates of the change in carbonate accumulation over the Neogene (Opdyke and Wilkinson, 1988; Delaney and Boyle, 1988; Mackenzie and Morse, 1992; Berner and Berner, 2012; Berner and Mackenzie, 2011; Dutkiewicz et al., 2018). If I assume that the hydrothermal and ion exchange fluxes do not change the estimated change in river input is $36 \pm 15\%$.

The results of changing carbonate input for a given shelf-basin partitioning value are impacted by pCO_2 . The early Miocene simulations consistently show that increasing pCO_2 for a given set of conditions deepens the position of the CCD slightly. Despite lower pH in Pacific deep water with increasing pCO_2 , abyssal $\text{CO}_3^{=}$ and calcite saturation both increase slightly with high pCO_2 . At higher pCO_2 DIC is significantly higher in the deep reservoirs, so both $\text{CO}_3^{=}$ and therefore calcite saturation increase slightly (Fig. 5).

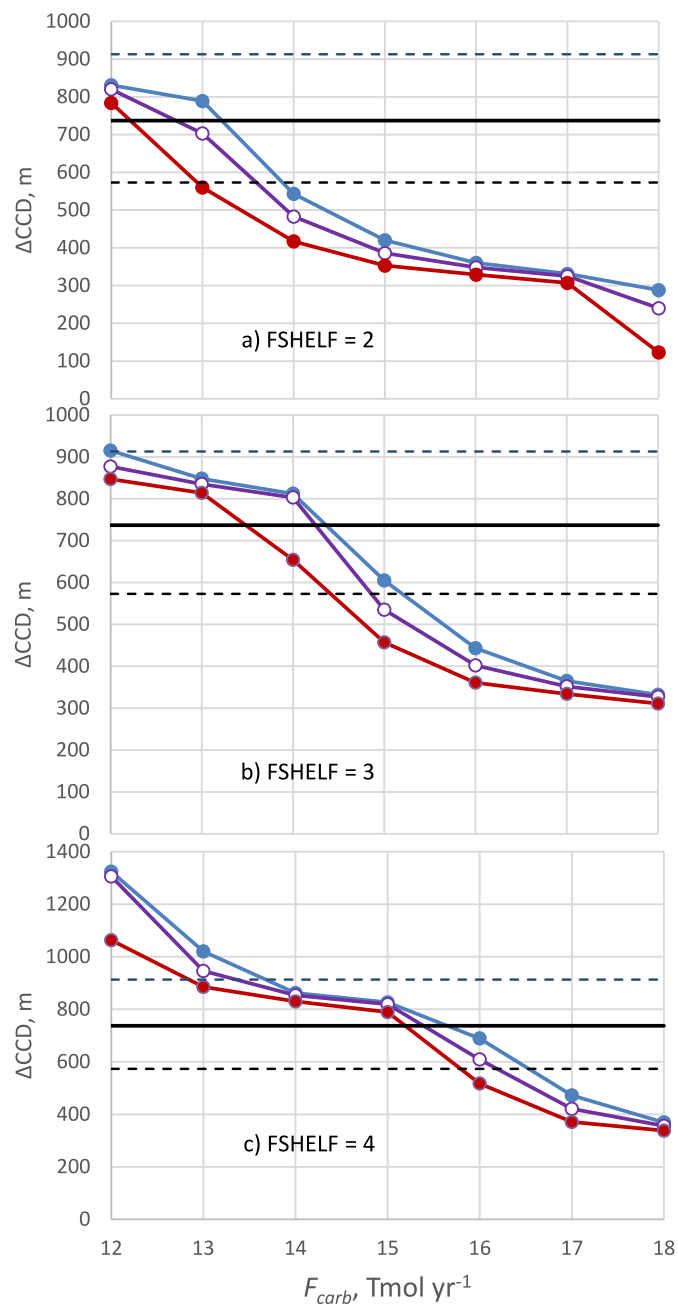


Fig. 4. a) LOSCAR simulation of deepening in Pacific CCD relative to modern case with FSHELF = 2. Model runs at 450 ppm (blue), 600 ppm (purple, open symbols), and 900 ppm (red). Black line is mean estimate of the change in Pacific CCD from Fig. 1 (Campbell et al., 2018), dashed lines are 95% C.I. b) Deepening in Pacific CCD relative to modern case with FSHELF = 3. Symbols same as 4a. c) Deepening in Pacific CCD relative to modern case with FSHELF = 4. Symbols same as 4a. Note change in vertical Δ CCD scale relative to 4a and 4b.

4.

4.1. Changes in total CO_2 in ocean-atmosphere system

At steady state atmospheric pCO_2 is controlled by DIC and alkalinity in the ocean. Around 50 times more CO_2 is present as dissolved DIC compared to atmospheric CO_2 and is available to exchange with the atmosphere on the time scale of oceanic mixing, ca. 1000 years. Any consideration of the change in atmospheric CO_2 over time must account for changes in DIC. The total CO_2 in the ocean-atmosphere system is

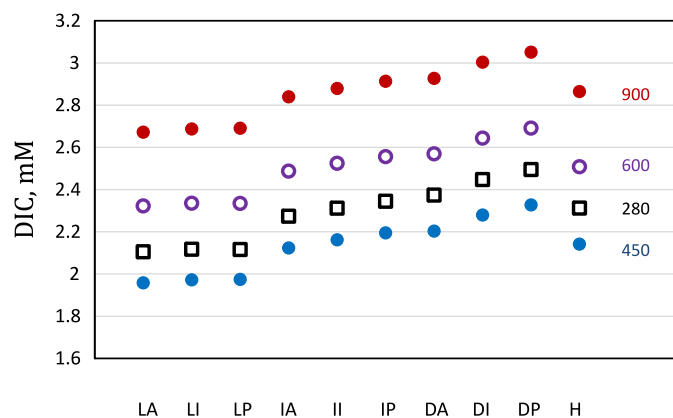


Fig. 5. Distribution of DIC in the ten LOSCAR oceanic reservoirs at different pCO_2 with constant modern shelf-basin partitioning and carbonate input (18 Tmol yr^{-1}). Estimated Miocene T and chemistry used for 450, 600 and 900 ppm. Modern conditions used for 280 ppm. Reservoirs: LA, LI, LP = surface Atlantic, Indian, Pacific. IA, II, IP = intermediate Atlantic, Indian, Pacific. DA, DI, DP = deep Atlantic, Indian, Pacific. H = high latitude.

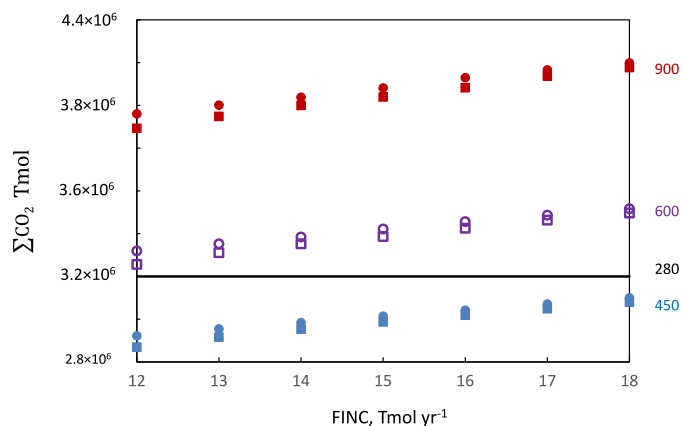


Fig. 6. Change in total atmosphere-ocean carbon (ΣCO_2) for different carbonate fluxes (FINC) and pCO_2 . Modern conditions (black horizontal line) calculated using FINC = 18 Tmol yr^{-1} and modern water column T and chemistry. All others use early Miocene estimates (Table 1). Round symbols for FSHELF = 3, square for FSHELF = 4. Reduced carbonate input results in lower ΣCO_2 . Varying shelf-basin partitioning has only minor impact on the results. Based on modeling the change in CCD over time it is likely that FINC was ca. 13 to 14 in the early Miocene. Using this lower value would in turn lower the estimated early Miocene ΣCO_2 .

$$1. \quad \Sigma \text{CO}_2 = \sum V_i \text{DIC}_i + \text{pCO}_2 \cdot \gamma$$

where V_i and DIC_i are the volumes and calculated DIC values of the ten ocean boxes and γ is the conversion from atmospheric pCO_2 in ppmv to moles ($1.78 \times 10^{14} \text{ mol/ppmv}$). Changes in the terrestrial biomass and soil carbon reservoirs are not considered because constraints on how these may have changed over the Neogene are limited.

I compare ΣCO_2 between modern conditions and early Miocene with varying carbonate input and pCO_2 . The maximum change in ΣCO_2 between 900 ppm early Miocene conditions and modern value is from $4.25 \times 10^{18} \text{ mol CO}_2$ to the modern value $3.20 \times 10^{18} \text{ mol CO}_2$, or a decrease of -33% (Fig. 6). More realistically assuming an early Miocene carbonate weathering flux 28% lower than modern, the change in ΣCO_2 is -20% from the early Miocene 900 ppm case. For 600 ppm and a 28% decrease in FINC the change in ΣCO_2 is -4.5% despite the more than factor of two change in pCO_2 . At 450 ppm with early Miocene temperatures and ion chemistry, ΣCO_2 is lower than the modern value because the increased DIC in the ocean reservoirs under modern conditions more

than offsets the decreased CO₂ mass in the atmosphere (see Table S3). Previous studies have also calculated that DIC in the major ocean reservoirs stayed near-constant or increased since the early Miocene when the effects of changes in seawater composition and *T* are included, notably the decline in Ca⁺⁺ concentration (Zeebe and Tyrrell, 2019). Sosdian et al. (2020) show a transient peak in surface ocean DIC associated with the MCO at 16 Ma, but otherwise little net change from 22 to 11 Ma. Boudreau et al. (2019) model a large increase (≈ 0.7 mM) in both surface and deep water DIC since 20 Ma. Caves et al., 2016 found a slight net increase of $\sum\text{CO}_2$ over the same time interval. At higher pCO₂ (600 and 900 ppm) we find higher oceanic DIC than modern even with early Miocene ocean temperatures and chemistry, and would thus require a small net decline in $\sum\text{CO}_2$ during the Neogene, similar to Roberts and Tripathi (2009) who modeled the effects of decreasing CO₂ from 556 to 278 ppm. The LOSCAR simulations find that less shelf deposition and more carbonate input both tend to increase deep water DIC and $\sum\text{CO}_2$ (as expected), but the effects are significantly smaller than those produced by changes in ion composition and pCO₂ (Fig. 6). For smaller changes in pCO₂ (from 450 to 280 ppm) the effect of changes in the ion chemistry of seawater outweighs the change in the mass of the smallest reservoir, the atmosphere. The moderate response of $\sum\text{CO}_2$ to larger changes in pCO₂ is partly a consequence of the deep ocean remaining near carbonate saturation under a range of plausible conditions (Zeebe and Westbroek, 2003; Boudreau et al., 2019). It is worth noting that unlike some previous models the simulations here do not impose fixed alkalinity, saturation state or CO₃⁼_{surf}/CO₃⁼_{deep}.

The modest relative change in the ocean atmosphere carbon reservoir over time is a strong constraint on weathering models. The mean rate of change of $\sum\text{CO}_2$ since 20 Ma varies from a maximum of -0.05 Tmol yr⁻¹ (from 900 ppm CO₂) to $+0.01$ Tmol yr⁻¹ (from 450 ppm). These values represent the mean annual imbalance between CO₂ inputs and outputs. They are small compared to the overall exogenic carbon fluxes of 25 Tmol yr⁻¹, or estimates of silicate weathering, taken here as near 7 Tmol yr⁻¹. The mean annual imbalance with respect to the silicate weathering flux is not more than -0.7% even for a large long-term decrease in atmospheric CO₂ from 900 to 280 ppm. Caves et al., 2016 came to a similar conclusion using a simplified model of ocean alkalinity and carbon balances with more restrictive assumptions. The present study and the others summarized here show that it is possible that the total ocean-atmosphere CO₂ inventory has increased from the mid-early Miocene to the present, and at most decreased only slightly. An increase or minimal decrease in $\sum\text{CO}_2$ is clearly at odds with a large body of literature (e.g. the influential work of Raymo and Ruddiman, 1992) that has in various ways invoked substantial weathering or organic carbon burial increases to explain an apparent drop in atmospheric pCO₂ and generally cooling climate over the Neogene.

The small change in net CO₂ balances constrained by this calculation implies that, whatever the source of the approximately 30% increased alkalinity flux was to the global ocean, it can only have been silicate weathering if there was a very closely matched increase in degassing over the same time interval. In that scenario a tightly coupled feedback could increase weathering fluxes. However, mechanistic models of climate-weathering feedback produce fluxes that scale positively with increased temperature. Global cooling since the early Miocene is not consistent with such a mechanism. LOSCAR uses a simple feedback that only depends on pCO₂, i.e. there is no explicit temperature feedback, but the model assumes that atmospheric pCO₂ is a suitable proxy for global temperature and precipitation, providing an implicit physical mechanism for a feedback relation. Consequently, the increase in alkalinity flux necessary to produce the observed fall in the CCD and increased global carbonate accumulation must be provided by

carbonate weathering. Caves Rugenstein et al., 2019 also modeled very little change in silicate weathering and a substantial increase in carbonate weathering fluxes since the mid-Miocene, but they found a much larger change (+30% to +340%). The results here only overlap with the lower part of the carbonate weathering increase they proposed, as 100% increases in carbonate weathering cannot be reconciled with the estimate of CCD changes unless a) there was essentially no change in shelf-basin partitioning despite changes in sea level and shelf area, and/or b) the Pacific CCD change from Campbell et al., 2018 is a significant underestimate and their less well constrained Indian Ocean record is more representative of the global response. At this point neither of those scenarios appear likely.

4.2. Role of pyrite weathering

The oxidation of pyrite and concomitant production of acidity can dissolve carbonate minerals and generate CO₂ that is not returned to the atmosphere on the time scale of carbonate precipitation in the oceans (Spence and Telmer, 2005). Consequently sulfide weathering can act as a source of CO₂ over time scales shorter than the response time of oceanic sulfate. The Cenozoic increase in seawater sulfate concentration (Horita et al., 2002; Brennan et al., 2013) provides some constraint on the global role of this process. Beginning with an early Miocene seawater sulfate concentration $[\text{SO}_4^{=}]_{\text{sw}} = 22 \pm 3$ mM, the increase to the modern value (28.3 mM) is 6.3 ± 3 mM, an average rate of increase = $4.4 \pm 2.1 \times 10^{11}$ mol yr⁻¹. This is a net rate balancing S inputs (primarily rivers) with S removal (sulfate reduction and removal of SO₄⁼ in carbonates and evaporites). Seawater $\delta^{34}\text{S}$ shows little variation during the Neogene (Paytan et al., 1998). The simplest explanation for this constancy is that fractional rates of sulfate reduction did not vary (this is not strictly required if offsetting fluxes change just enough to maintain constant seawater $\delta^{34}\text{S}$). With this assumption and an approximate 1:1 SO₄⁼/CO₂ ratio, CO₂ production rates via sulfide weathering are maximally ≈ 0.44 Tmol yr⁻¹ if all the increase in seawater SO₄⁼ results from terrestrial pyrite oxidation. In areas of high relief, the fraction of river SO₄⁼ derived from pyrite oxidation has been estimated at of 67–100% (Spence and Telmer, 2005; Calmels et al., 2007; Kemeny et al., 2021) whereas global estimates are $46 \pm 7\%$ (Burke et al., 2018). Thus a more realistic estimate of the mean CO₂ production rate over the Neogene from sulfide oxidation is ≈ 0.20 Tmol C yr⁻¹. That CO₂ production flux is 2.9% of the global rate of CO₂ consumption via silicate weathering used here.

5. Discussion

5.1. Increased alkalinity fluxes reflected in CCD deepening

The deepening of the CCD since the early Miocene implies an increase in carbonate alkalinity fluxes to the oceans over the last 20–25 Ma. Here we obtain an increase of $28 \pm 12\%$ as a plausible estimate of the increase in the total carbonate flux to the oceans (river flux change $36 \pm 15\%$ if other sources remain fixed) with the value dependent on a) the extent of change in shelf-basin partitioning, b) change in pCO₂, and c) changes in major ion chemistry and temperature of the oceans via their impact on carbonate system parameters. A larger range in allowable solutions is possible if the above terms are varied more widely, but changes in the parameter with the single largest influence, shelf-basin partitioning, cannot be less than zero relative to a low mean Pleistocene sea level or more than an ice free world would permit. I show that an idealized analytical model is consistent with the results of numerical modeling using LOSCAR. The estimated increase in carbonate weathering flux is also consistent with $\delta^{13}\text{C}$ mass balances over

the same interval, but uncertainties in the carbon isotope mass balance mean that the $\delta^{13}\text{C}$ data do not tightly constrain changes in the carbonate flux. Uncertainties remain in the extent of CCD change, in part from the necessity of correcting important Pacific sites for paleodepth changes resulting from dynamic topography variations (Campbell et al., 2018). The LOSCAR simulations also do not effectively capture the observed greater CCD deepening in the Indian ocean; the cause and significance of this disagreement is not clear. The *ca.* 30% increase in carbonate flux to and therefor carbonate deposition in the oceans is broadly similar to several previous studies (Opdyke and Wilkinson, 1988; Berner and Berner, 2012; Berner and Mackenzie, 2011; Dutkiewicz et al., 2018; Boudreau et al., 2019). Carbon isotope mass balances over the Neogene are fully consistent with increased carbonate fluxes (Delaney and Boyle, 1988), but do not provide a particularly tight constraint on the system and so are not addressed further here. A discussion of this issue is in the SI.

5.2. Modest changes in total ocean-atmosphere carbon

Consistent with several other studies (Zeebe and Tyrrell, 2019; Roberts and Tripathi, 2009; Caves et al., 2016; Boudreau et al., 2019), the simulations find modest and possibly positive changes in oceanic DIC since the early Miocene despite decreasing atmospheric $p\text{CO}_2$. Given that a variety of differently constructed models produce this result it is a robust finding that places strong and important constraints on models of the carbon balance in the ocean-atmosphere system. The effect of changing seawater temperatures and chemistry is such that, for early Miocene $p\text{CO}_2$ of 450 ppm, the total ocean-atmosphere carbon $\sum\text{CO}_2$ is smaller than the pre-anthropogenic modern value, highlighting the influence of seawater chemical changes on CO_2 distribution (e.g. Zeebe and Tyrrell, 2019; Hain et al., 2015; Sosdian et al., 2020). Models that assume higher early-mid-Miocene $p\text{CO}_2$ do produce a net decline in $\sum\text{CO}_2$ to the modern value, but the change is not large and implies a mean annual net imbalance in long term CO_2 (production – consumption) $\leq -0.7\%$ for $p\text{CO}_2$ as high as 900 ppm, with zero net imbalance or even a small positive balance as allowable solutions, as previously argued by Caves et al. (2016). We also note that the inversion results of Boudreau et al. (2019) imply a large positive change (30%) in $\sum\text{CO}_2$ since 20 Ma. Because the calculations here represent net changes over the last 20 Ma, they do not preclude geologically short intervals when $\sum\text{CO}_2$ changed more rapidly, such as the MCO (Sosdian et al., 2020). Nor do they preclude changes in both degassing or organic carbon oxidation (the main inputs of CO_2) as long as they are almost always tightly coupled to changes in weathering and/or organic carbon burial such that the net flux changes little. It does however preclude models that call for progressive increase in net weathering fluxes to drive down CO_2 over the Neogene. A modest increase in silicate weathering consumption of CO_2 remains viable if net oxidation of the sedimentary organic carbon reservoir offsets such a change, but such an offset would have to be rather precise. Pyrite oxidation and consequent production of CO_2 can offset around 3% of CO_2 consumption by silicate weathering over the last 20 Ma. If that fractional contribution changed it could allow some slight decoupling between degassing and weathering rates, but the timing, magnitude and even sign of such a change is currently not clear. Similarly, if the sedimentary organic carbon reservoir experienced net growth over this interval (Derry and France-Lanord 1996), that would almost certainly require that net consumption of CO_2 via silicate weathering declined by near the same amount over the same interval. Such a decline would be consistent with decreasing $p\text{CO}_2$ and global temperatures.

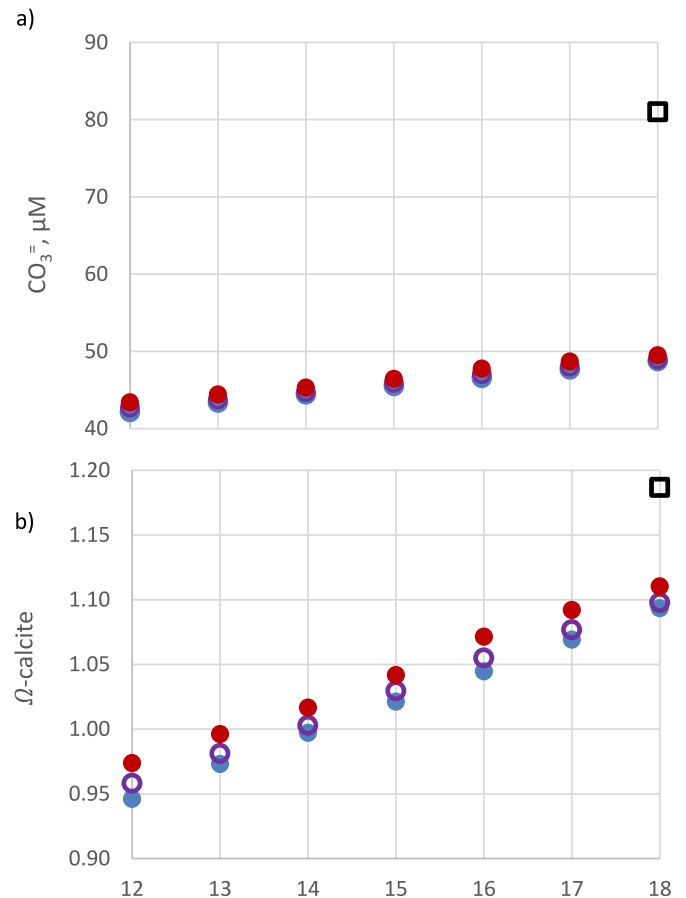


Fig. 7. a) Carbonate ion concentration in the deep Pacific reservoir for modern (black square) and early Miocene conditions as a function of weathering input flux. Miocene results for FSHELF = 3, early Miocene T and ion chemistry. Symbols for 450, 600 and 900 ppm CO_2 as in Fig. 6. The difference in major ion composition results in large increase in CO_3^{2-} for modern conditions. Increasing FINC has a smaller positive effect on CO_3^{2-} concentrations. b) Calcite saturation index in deep Pacific reservoir for modern (black square) and early Miocene conditions as a function of weathering input flux. Increasing FINC impacts Ω -calcite as does the change in ion composition from early Miocene to modern conditions. The value for Ω -calcite is an average across the depth range of the deep reservoir computed by LOSCAR. The increased in average Ω -calcite indicates increasing carbonate saturation overall in the deep Pacific, consistent with a deepening of the CCD, but this representation does not resolve the depth variation in saturation state.

5.3. Stable Neogene $\sum\text{CO}_2$ and the causes of $p\text{CO}_2$ decline

The apparent paradox of small changes in $\sum\text{CO}_2$ and large changes in $p\text{CO}_2$ over the Neogene suggests an internal mechanism for $p\text{CO}_2$ change. Carbonate ion concentration in all the ocean reservoirs is significantly higher for modern conditions than for any of the Miocene scenarios (Fig. 7 shows differences for the deep Pacific). This difference shows little dependence on FSHELF, and weak dependence on FINC. The major difference is the major ion composition of seawater, with Ca^{++} declining from early Miocene values of 14–15 to near 10 mM (Horita et al., 2002; Brennan et al., 2013). The tendency for deep water to approach calcite saturation therefore implies a large increase in CO_3^{2-} (Zeebe and Tyrrell, 2019). Model results show that carbonate ion in the deep Pacific reservoir increases from early Miocene values $\approx 45 \mu\text{M}$ to $> 80 \mu\text{M}$ (Fig. 7a). The same effect propagates through the intermediate and surface reservoirs, for example CO_3^{2-} in the surface Pacific increases from *ca.* 180 to 260 μM from Miocene to modern conditions (see SI). The result is a decrease in the DIC/TALK ratio which results in increased solubility of CO_2 , lowering $p\text{CO}_2$ (Fig. 8). Calcite saturation in the deep ocean also increases with the change

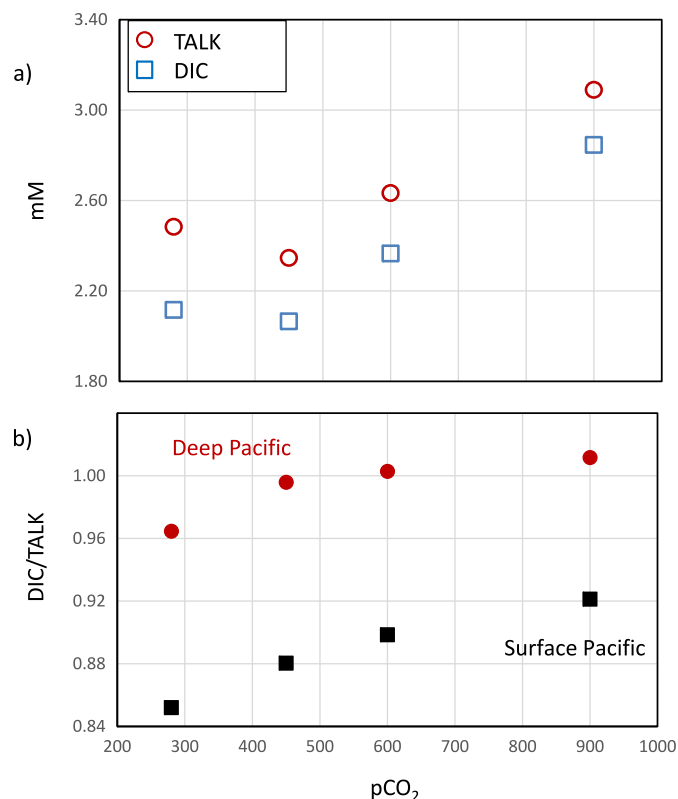


Fig. 8. a) Computed Pacific surface water DIC and TALK (total alkalinity) for modern values of shelf-basin partitioning FS_{SHELF} and carbonate input $FINC = 18 \text{ Tmol yr}^{-1}$. 280 ppm calculated with modern ocean conditions; 450, 600 and 900 ppm calculated with early Miocene conditions similar to Fig. 6. DIC and TALK are lower for 450 ppm case than for modern (280 ppm). b) Atmospheric $p\text{CO}_2$ sensitively reflects changes in the surface ocean DIC/TALK ratio (see also Figure S4). The surface Pacific reservoir is plotted here because it has the largest surface area but the Indian and Atlantic have the same DIC/TALK. The deep Pacific reservoir also shows progressive decrease in DIC/TALK for decreasing $p\text{CO}_2$. DIC/TALK ratios are not sensitive to changes in carbonate inputs or shelf-basin partitioning.

in ion composition but is also dependent on the carbonate weathering input (Fig. 7b).

The major driver for the difference between high early Miocene $p\text{CO}_2$ and lower modern values is not a change in the total CO_2 in the ocean atmosphere system, but a redistribution of that CO_2 from the atmosphere to the ocean. This is reflected in the calculated atmospheric fraction of $\sum\text{CO}_2$, which was 2.7 to 4.1% for early Miocene $p\text{CO}_2$ (450–900 ppm, see SI) but decreased to 1.6% for modern conditions. Increased carbonate weathering flux has a smaller impact by increasing overall deep water saturation state. Although we do not know $p\text{CO}_2$ at the start of the Neogene particularly precisely, a significant decline to pre-anthropogenic values requires small or even zero change in the overall carbon budget of the ocean atmosphere. This is a fundamentally different view of the causes for Neogene $p\text{CO}_2$ variation than commonly invoked mechanisms of degassing-weathering or organic carbon cycle imbalances that would achieve $p\text{CO}_2$ changes by altering the overall stock of carbon.

The Neogene decline in Ca^{++} and Ca/Mg is consistent with decreased low T alteration of the oceanic crust (Coggon et al., 2010). Reduced low T alteration also reduces acidity generation, i.e. the rate of alkalinity removal (Spivack and Staudigel, 1994), further helping to lower the DIC/TALK ratio. The decreased rate of low T alteration could be a function of lower deep ocean temperatures (Coogan and Dosso, 2015; Coogan and Gillis, 2018). In that case a positive feedback may arise with cooler ocean temperatures leading to lower Ca^{++} via reduced Mg exchange, which in turn leads

to high $\text{CO}_3^{=}$ and lower DIC/TALK, driving decreased $p\text{CO}_2$. This positive feedback may offset any negative feedback of cooler temperatures on carbonate weathering.

6. Summary

This study has focused on variables that are directly tied to the oceanic carbon system and can be estimated, if imperfectly, from the paleoceanographic record. They are the CCD, $p\text{CO}_2$, and the major ion composition of seawater. I used the LOSCAR ocean carbon model and compared steady state solutions for the ocean carbon system with estimates of early Miocene conditions to modern pre-anthropogenic conditions. Because the solutions are steady state they do not provide constraints on the path between early Miocene and modern conditions, but they do provide insight into the overall nature of the changes and what processes could drive them. I find two principal results.

The net result of tectonic and climate processes on carbon fluxes over the last 20–25 Ma can be summarized as a carbonate weathering event, with carbonate weathering fluxes increasing over time. Neogene changes in marine carbonate deposition essentially reflect weathering of carbonate rocks and redeposition as marine sediment, modulated by variations in shelf-basin partitioning. The tectonic conversion of the carbonate-rich Tethyan margin to mountain ranges from the Anti-Atlas to the Himalaya is one plausible driver of increased carbonate weathering over the Neogene. Currently 41% of carbonate outcrop occurs in mountainous regions (Goldscheider et al., 2020), and an important fraction of this is distributed along active or former convergent margins from Iberia to SE Asia. While the response of carbonate weathering to tectonic forcing may be complex, floodplain weathering of detrital carbonate probably plays a key role (Lupker et al., 2012; Erlanger et al., 2021). A more detailed reconstruction of carbonate weathering fluxes and the processes that control them over time is needed to test this hypothesis.

Using parameters that directly reflect the carbon cycle to constrain changes in the amount and distribution of carbon in the ocean atmosphere system, the results here show room for, at most, only slight net changes in carbon content of the ocean-atmosphere system over the Neogene. On average silicate weathering fluxes differed little from CO_2 inputs, and even the sign of the long-term trend in the overall late Cenozoic carbon balance is not certain, implying a limited role for tectonic forcing of silicate weathering. However, I do find evidence for substantial and redistribution of carbon from the atmosphere to the oceans, with the potential to drive large decreases in atmospheric $p\text{CO}_2$ with negligible changes in the overall ocean atmosphere mass balance for carbon. I hypothesize that the observed decrease in seawater Ca^{++} is a major driver for this change, with a smaller role for an enhanced carbonate weathering input. Increased (or even constant) deep ocean saturation with the observed decline in Ca^{++} levels straightforwardly implies large increases in $\text{CO}_3^{=}$, resulting in increased CO_2 solubility. The consequent decrease in the DIC/TALK ratio of the ocean reservoirs can drive substantial reductions in $p\text{CO}_2$. More detailed non-steady state modeling of the Neogene ocean-atmosphere carbon budget can further test this hypothesis, and improved records of seawater composition through time could be very valuable. The view that redistribution of CO_2 from the atmosphere to the ocean at near-constant total carbon inventory is the primary cause of Neogene $p\text{CO}_2$ change represents a significant change in paradigm from models that primarily rely on silicate degassing-weathering or organic carbon oxidation-burial imbalances to drive changes in size of the ocean-atmosphere C reservoir. The potential feedback between cooling deepwater T, changing rates of low temperature OC alteration, lower seawater Ca^{++} ion concentration and falling $p\text{CO}_2$ presents a new working hypothesis for late Cenozoic cooling.

CRediT authorship contribution statement

Louis Derry: Conceptualization, modeling and writing.

Declaration of competing interest

The authors declare that they have no known competing financial interests or personal relationships that could have appeared to influence the work reported in this paper.

Data availability

No data was used for the research described in the article.

Acknowledgements

This work was supported by the French program Investissements Pour l'Avenir under ANR-17-MPGA-0009. Thanks to Steve Clemens (Brown University) for advice on late Cenozoic stable isotope records and to Richard Zeebe (University of Hawaii) for sharing the LOSCAR code and providing advice on setting it up. Any errors are, however, the sole responsibility of the author. Insightful review comments from Jeremy Caves-Rugenstein and an anonymous reader and from Editor Andy Jacobson spurred me to refine and clarify the ms. in important ways.

Appendix A. Supplementary material

Supplementary material related to this article can be found online at <https://doi.org/10.1016/j.epsl.2022.117801>.

References

- Amante, C., Eakins, B.W., 2009. ETOPO1 1 Arc-Minute Global Relief Model: Procedures, Data Sources and Analysis. NOAA Technical Memorandum NESDIS NGDC-24.
- Archer, D., 1996. An atlas of the distribution of calcium carbonate in sediments of the deep sea. *Glob. Biogeochem. Cycles* 10 (1), 159–174.
- Berner, E.K., Berner, R.A., 2012. *Global Environment: Water, Air, and Geochemical Cycles*, second ed. Princeton University Press, Princeton, NJ.
- Berner, R.A., Mackenzie, F.T., 2011. Burial and preservation of carbonate rocks over Phanerozoic time. *Aquat. Geochem.* 17, 727–733. <https://doi.org/10.1007/s10498-010-9113-0>.
- Boss, S.K., Wilkinson, B.H., 1991. Planktonic/eustatic control on cratonic/oceanic carbonate accumulation. *J. Geol.* 99, 497–513. <https://doi.org/10.1086/629513>.
- Boudreau, B.P., Luo, Y., 2017. Retrodiction of secular variations in deep-sea CaCO₃ burial during the Cenozoic. *Earth Planet. Sci. Lett.* 474, 1–12. <https://doi.org/10.1016/j.epsl.2017.06.005>.
- Boudreau, B.P., Middelburg, J.J., Sluifs, A., van der Ploeg, R., 2019. Secular variations in the carbonate chemistry of the oceans over the Cenozoic. *Earth Planet. Sci. Lett.* 512, 194–206. <https://doi.org/10.1016/j.epsl.2019.02.004>.
- Brennan, S.T., Lowenstein, T.K., Cendon, D.I., 2013. The major-ion composition of Cenozoic seawater: the past 36 million years from fluid inclusions in marine halite. *Am. J. Sci.* 313, 713–775.
- Burls, N.J., Bradshaw, C.D., De Boer, A.M., Herold, N., Huber, M., et al., 2021. Simulating Miocene warmth: insights from an opportunistic multi-model ensemble (MioMIP1). *Paleoceanogr. Paleoclimatol.* 36, e2020PA004054. <https://doi.org/10.1029/2020PA004054>.
- Burke, A., Present, T.M., et al., 2018. Sulfur isotopes in rivers: insights into global weathering budgets, pyrite oxidation, and the modern sulfur cycle. *Earth Planet. Sci. Lett.* 496, 168–177. <https://doi.org/10.1016/j.epsl.2018.05.022>.
- Calmels, D., Gaillardet, J., Brenot, A., France-Lanord, C., 2007. Sustained sulfide oxidation by physical erosion processes in the Mackenzie River basin: climatic perspectives. *Geology* 35 (11), 1003–1006.
- Campbell, S.M., Moucha, R., Derry, L.A., Raymo, M.E., 2018. Effects of dynamic topography on the Cenozoic carbonate compensation depth. *Geochim. Geophys. Res.* 19. <https://doi.org/10.1002/2017GC007386>.
- Cartapanis, O., Galbraith, E.D., Bianchi, D., Jaccard, S.L., 2018. Carbon burial in deep-sea sediment and implications for oceanic inventories of carbon and alkalinity over the last glacial cycle. *Clim. Past* 14, 1819–1850. <https://doi.org/10.5194/cp-14-1819-2018>.
- Caves, J.K., Jost, A.B., Lau, K.V., Maher, K., 2016. Cenozoic carbon cycle imbalances and a variable weathering feedback. *Earth Planet. Sci. Lett.* 450, 152–163. <https://doi.org/10.1016/j.epsl.2016.06.035>.
- Caves Rugenstein, J.K., Ibarra, D.E., von Blanckenburg, F., 2019. Neogene cooling driven by land surface reactivity rather than increased weathering fluxes. *Nature* 571, 99–102. <https://doi.org/10.1038/s41586-019-1332-y>.
- Coggon, R.M., Teagle, D.A.H., Smith-Duque, C.E., Alt, J.C., Cooper, M.J., 2010. Reconstructing past seawater Mg/Ca and Sr/Ca from mid-ocean ridge flank calcium carbonate veins. *Science* 327, 1114–1117.
- Coogan, L.A., Dosso, S.E., 2015. Alteration of ocean crust provides a strong temperature dependent feedback on the geological carbon cycle and is a primary driver of the Sr-isotopic composition of seawater. *Earth Planet. Sci. Lett.* 415, 38–46. <https://doi.org/10.1016/j.epsl.2015.01.027>.
- Coogan, L.A., Gillis, K.M., 2018. Temperature dependence of chemical exchange during seafloor weathering: insights from the Troodos ophiolite. *Geochim. Cosmochim. Acta* 243, 24–41. <https://doi.org/10.1016/j.gca.2018.09.025>.
- Cramer, B.S., Miller, K.G., Barrett, P.J., Wright, J.D., 2011. Late Cretaceous–Neogene trends in deep ocean temperature and continental ice volume: reconciling records of benthic foraminiferal geochemistry ($\delta^{18}\text{O}$ and Mg/Ca) with sea level history. *J. Geophys. Res., Oceans* 116 (C12), C12023. <https://doi.org/10.1029/2011JC007255>.
- Delaney, M.L., Boyle, E.A., 1988. Tertiary paleoceanic chemical variability: unintended consequences of simple geochemical models. *Paleoceanography* 3 (2), 137–156. <https://doi.org/10.1029/PA003i02p0137>.
- Dutkiewicz, A., Muller, R.D., Cannon, J., Vaughan, S., Zahirovic, S., 2018. Sequestration and subduction of deep-sea carbonate in the global ocean since the Early Cretaceous. *Geology*. <https://doi.org/10.1130/G45424.1>.
- Dutkiewicz, A., Müller, R.D., 2021. The carbonate compensation depth in the South Atlantic Ocean since the Late Cretaceous. *Geology* 49, 873–878. <https://doi.org/10.1130/G48404.1>.
- Erlanger, E.D., Rugenstein, J.K.C., Bufe, A., Picotti, V., Willett, S.D., 2021. Controls on physical and chemical denudation in a mixed carbonate-siliciclastic orogen. *J. Geophys. Res., Earth Surf.* 126, e2021JF006064. <https://doi.org/10.1029/2021JF006064>.
- Farrell, J.W., Prell, W.L., 1991. Pacific CaCO₃ preservation and $\delta^{18}\text{O}$ since 4 Ma: paleoceanic and paleoclimatic implications. *Paleoceanography* 6, 485–498.
- France-Lanord, C., Derry, L.A., 1997. Organic carbon burial forcing of the carbon cycle from Himalayan erosion. *Nature* 390, 65–67.
- Hain, M.P., Sigman, D.M., Higgins, J.A., Haug, G.H., 2015. The effects of secular calcium and magnesium concentration changes on the thermodynamics of seawater acid/base chemistry: implications for Eocene and Cretaceous ocean carbon chemistry and buffering. *Glob. Biogeochem. Cycles* 29. <https://doi.org/10.1002/2014GB004986>.
- Horita, J., Zimmermann, H., Holland, H.D., 2002. Chemical evolution of seawater during the Phanerozoic: implications for the record of marine evaporites. *Geochim. Cosmochim. Acta* 66 (21), 3733–3756.
- Iglesias-Rodríguez, M., Armstrong, R., Feely, R., Hood, R., Kleypas, J., Milliman, J.D., Sabine, C., Sarmiento, J., 2002. Progress made in study of ocean's calcium carbonate budget. *Eos* 83 (34), 365, 374–375.
- Gaillardet, J., Dupré, B., Louvat, P., Allègre, C.J., 1999. Global silicate weathering and CO₂ consumption rates deduced from the chemistry of large rivers. *Chem. Geol.* 159 (1–4), 3–30. [https://doi.org/10.1016/S0009-2541\(99\)00031-5](https://doi.org/10.1016/S0009-2541(99)00031-5).
- Goldschneider, N., Chen, Z., Auler, A.S., Bakalowicz, M., Broda, S., Drew, D., Hartmann, J., Jiang, G., Moosdorf, N., Stevanovic, Z., Veni, G., 2020. Global distribution of carbonate rocks and karst water resources. *Hydrogeol. J.* 28, 1661–1677. <https://doi.org/10.1007/s10040-020-02139-5>.
- Gothmann, A.M., Stolarski, J., Adkins, J.F., Schoene, B., Dennis, K.J., Scharg, D.P., Mazur, M., Bender, M.L., 2015. Fossil corals as an archive of secular variations in seawater chemistry since the Mesozoic. *Geochim. Cosmochim. Acta* 160, 188–208. <https://doi.org/10.1016/j.gca.2015.03.018>.
- Kemeny, P.C., Lopez, G.L., Dalleska, N.F., Torres, M., Burke, A., Bhatt, M.P., West, A.J., Hartmann, J., Adkins, J.F., 2021. Sulfate sulfur isotopes and major ion chemistry reveal that pyrite oxidation counteracts CO₂ drawdown from silicate weathering in the Langtang-Trisuli-Narayani River system, Nepal Himalaya. *Geochim. Cosmochim. Acta* 294, 43–69. <https://doi.org/10.1016/j.gca.2020.11.009>.
- Komar, N., Zeebe, R., 2021. Reconciling atmospheric CO₂, weathering, and calcite compensation depth across the Cenozoic. *Sci. Adv.* 7, eabd4876.
- Lear, C.H., Coxall, H.K., Foster, G.L., Lunt, D.J., Mawbey, E.M., Rosenthal, Y., Sosdian, S.M., Thomas, E., Wilson, P.A., 2015. Neogene ice volume and ocean temperatures: Insights from infaunal foraminiferal Mg/Ca paleothermometry. *Paleoceanography* 30, 1437–1454. <https://doi.org/10.1002/2015PA002833>.
- Lupker, M., France-Lanord, C., Galy, V., Lavé, J., Gaillardet, J., Gajurel, A.P., Guilmette, C., Rahman, M., Singh, S.K., Sinha, R., 2012. Predominant floodplain over mountain weathering of Himalayan sediments (Ganga basin). *Geochim. Cosmochim. Acta* 84, 410–432. <https://doi.org/10.1016/j.gca.2012.02.001>.
- Lyle, M., 2003. Neogene carbonate burial in the Pacific Ocean. *Paleoceanography* 18 (3), 1059. <https://doi.org/10.1029/2002PA000777>.
- Mackenzie, F.T., Morse, J.W., 1992. Sedimentary carbonates through Phanerozoic time. *Geochim. Cosmochim. Acta* 56, 3281–3295.
- Miller, K.G., Browning, J.V., Schmelz, J., Kopp, R.E., Mountain, G.S., Wright, J.D., 2020. Cenozoic sea-level and cryospheric evolution from deep-sea geochemical and continental margin records. *Sci. Adv.* 6, eaaz1346.

- Opdyke, B.N., Wilkinson, B.H., 1988. Surface area control of shallow cratonic to deep marine carbonate accumulation. *Paleoceanography* 3 (6), 685–703. <https://doi.org/10.1029/PA003i006p00685>.
- Pälike, H., Lyle, M.W., et al., 2012. A Cenozoic record of the equatorial Pacific carbonate compensation depth. *Nature* 488, 609–614. <https://doi.org/10.1038/nature11360>.
- Paytan, A., Kastner, M., Campbell, D., Thiemens, M.H., 1998. Sulfur isotopic composition of Cenozoic seawater sulfate. *Science* 282, 1459–1462. <https://doi.org/10.1126/science.282.5393.1459>.
- Peterson, L.C., Backman, J., 1990. Late Cenozoic carbonate accumulation and the history of the carbonate compensation depth in the western equatorial Indian Ocean. *Proc. Ocean Drill. Program Sci. Results* 115, 467–507.
- Rae, J.W.B., Zhang, Y.G., Liu, X., Foster, G.L., Stoll, H.M., Whiteford, R.D.M., 2021. Atmospheric CO₂ over the past 66 million years from marine archives. *Annu. Rev. Earth Planet. Sci.* 49, 609–641. <https://doi.org/10.1146/annurev-earth-082420-063026>.
- Rausch, S., Böhm, F., Bach, W., Klügel, A., Eisenhauer, A., 2012. Calcium carbonate veins in ocean crust record a threefold increase of seawater Mg/Ca in the past 30 million years. *Earth Planet. Sci. Lett.* 362, 215–224. <https://doi.org/10.1016/j.epsl.2012.12.00>.
- Raymo, M.E., Ruddiman, W.F., 1992. Tectonic forcing of late Cenozoic climate. *Nature* 359, 117–122.
- Roberts, C.D., Tripathi, A., 2009. Modeled reconstructions of the oceanic carbonate system for different histories of atmospheric carbon dioxide during the last 20 Ma. *Glob. Biogeochem. Cycles* 23, GB1011. <https://doi.org/10.1029/2008GB003310>.
- Rowley, D.B., Forte, A.M., Rowan, C.J., Glisovic, P., Moucha, R., Grand, S.P., Simmons, N.A., 2016. Kinematics and dynamics of the East Pacific Rise linked to a stable, deep-mantle upwelling. *Sci. Adv.* 2, e1601107.
- Si, W., Rosenthal, Y., 2019. Reduced continental weathering and marine calcification linked to late Neogene decline in atmospheric CO₂. *Nat. Geosci.* 12, 833–838. <https://doi.org/10.1038/s41561-019-0450-3>.
- Sosdian, M., Babila, T.L., Greenop, R., Foster, G.L., Lear, C.H., 2020. Ocean carbon storage across the middle Miocene: a new interpretation for the Monterey Event. *Nat. Commun.* 11, 134. <https://doi.org/10.1038/s41467-019-13792-0>.
- Spence, J., Telmer, K., 2005. The role of sulfur in chemical weathering and atmospheric CO₂ fluxes: evidence from major ions, $\delta^{13}\text{C}_{\text{DIC}}$, and $\delta^{34}\text{S}_{\text{SO}_4}$ in rivers of the Canadian Cordillera. *Geochim. Cosmochim. Acta* 69 (23), 5441–5458.
- Spivack, A.J., Staudigel, H., 1994. Low-temperature alteration of the upper oceanic crust and the alkalinity budget of seawater. *Chem. Geol.* 115, 239–247.
- Steinthorsdottir, M., Coxall, H.K., de Boer, A.M., Huber, M., Barbolini, N., Bradshaw, C.D., et al., 2021. The Miocene: the future of the past. *Paleoceanogr. Paleoclimatol.* 36, e2020PA004037. <https://doi.org/10.1029/2020PA004037>.
- Suchéras-Marx, B., Henderiks, J., 2014. Downsizing the pelagic carbonate factory: impacts of calcareous nannoplankton evolution on carbonate burial over the past 17 million years. *Glob. Planet. Change* 123, 97–109. <https://doi.org/10.1016/j.gloplacha.2014.10.015>.
- Tyrrell, T., Zeebe, R.E., 2004. History of carbonate ion concentration over the last 100 million years. *Geochim. Cosmochim. Acta* 68 (17), 3521–3530.
- Van Andel, T.H., 1975. Mesozoic/Cenozoic calcite compensation depth and the global distribution of calcareous sediments. *Earth Planet. Sci. Lett.* 26 (2), 187–194. [https://doi.org/10.1016/0012-821X\(75\)90086-2](https://doi.org/10.1016/0012-821X(75)90086-2).
- Zeebe, R.E., Zachos, J.C., Dickens, G.R., 2009. Carbon dioxide forcing alone insufficient to explain Paleocene-Eocene thermal maximum warming. *Nat. Geosci.* 2, 576–580. <https://doi.org/10.1038/NGEO578>.
- Zeebe, R.E., 2012. LOSCAR: long-term ocean-atmosphere sediment carbon cycle reservoir model v20.4. *Geosci. Model Dev.* 5, 149–166.
- Zeebe, R.E., Tyrrell, T., 2019. History of carbonate ion concentration over the last 100 million years II: revised calculations and new data. *Geochim. Cosmochim. Acta* 257, 373–392. <https://doi.org/10.1016/j.gca.2019.02.041>.
- Zeebe, R.E., Westbroek, P., 2003. A simple model for the CaCO₃ saturation state of the ocean: the “Strangelove,” the “Neritan,” and the “Cretan” Ocean. *Geochem. Geophys. Geosyst.* 4 (12), 1104. <https://doi.org/10.1029/2003GC000538>.